Origin of noncollinear magnetization coupling across Ru*X* layers

Claas Abert [1,2,*] Sabri Koraltan [1,†] Florian Bruckner,[1] Florian Slanovc [1] Juliana Lisik [3] Pavlo Omelchenko,[3]
Erol Girt,[3] and Dieter Suess[1,2]

[1]*Faculty of Physics, University of Vienna, 1090 Vienna, Austria*
[2]*Research Platform MMM Mathematics-Magnetism-Materials, University of Vienna, 1090 Vienna, Austria*
[3]*Simon Fraser University, 8888 University Drive, Burnaby, British Columbia, V5A 1S6 Canada*

We present a simple atomistic model for the description of noncollinear coupling in magnetic multilayers with hybrid spacer layers made of Ru alloyed to ferromagnetic atoms such as Fe. In contrast to previous analytical and micromagnetic models that explain the noncollinear coupling by means of lateral fluctuations in the coupling constant, the presented model accounts for atom-atom coupling in all three spatial dimensions within the spacer layer. The model is able to accurately predict the dependence of the macroscopic bilinear and biquadratic coupling constants on the spacer-layer composition and thickness, showing much better quantitative agreement than lateral-fluctuation models. Moreover, it predicts that the noncollinear coupling is virtually independent of the exchange stiffness in the ferromagnetic layers, which goes beyond the predictions of previous models. This prediction is validated by experimental measurements.

I. INTRODUCTION

Magnetic multilayers build the backbone of many spintronics applications, such as magnetoresistive sensors [1,2], magnetoresistive random access memory (MRAM) [3–7], or spin-torque nano-oscillators [8–10]. The coupling between the magnetic layers plays a crucial role in controlling the functionality of multilayer devices. In this regard, an important effect is the Ruderman-Kittel-Kasuya-Yosida (RKKY) coupling [11], which introduces an exchange coupling between two magnetic layers separated by a nonmagnetic layer, typically made of Ru. Depending on the thickness of the nonmagnetic spacer layer, the RKKY coupling between the magnetic layers is either of a parallel or antiparallel nature and hence collinear. While a collinear coupling mechanism is useful, e.g., for the construction of synthetic antiferromagnets, a tunable control of the coupling angle would introduce numerous advantages for the design of spintronic devices.

Considering a typical spin-transfer torque MRAM device, as depicted in Fig. 1(a), the collinear alignment of the distinct magnetic layers introduces serious drawbacks to the writing process. Namely, the spin torque generated by a reference layer on a perfectly collinear free layer vanishes for the equilibrium configuration. In this case, the switching of the free layer is facilitated by thermal activation. By breaking the

collinearity between the reference layer and the free layer, this restriction is overcome, allowing for a reliable switching process with low power consumption.

A possible method to avoid collinearity in spin-torque devices is the tilting of the reference layer anisotropy [12,13]. Alternative strategies for noncollinear spin polarization include the use of two reference layers, one being in-plane and the other being out-of-plane [14,15], or the combination of an out-of-plane spin-polarization layer with an in-plane free layer [16,17]. In addition to the enhancement of MRAM performance, noncollinear magnetic multilayers have already been proven to be beneficial for spin-torque oscillators [18–20] and are likely to play a crucial role for designing a variety of future spintronic devices. Recently, a novel mechanism for the noncollinear coupling in magnetic multilayers was experimentally demonstrated [21], and it was shown that spacer layers made of RuFe alloys are able to generate a strong noncollinear coupling between two Co layers. The angle of this coupling can be precisely controlled by adjusting the ratio of the RuFe composition in the spacer layer. This introduces a very powerful tool for the development of novel spintronic devices. Figure 1(b) depicts an MRAM structure with noncollinear alignment between the free and reference layers, which is achieved by using a reference layer that consists of two noncollinearly coupled magnetic layers. Such a reference system would allow for a tilted spin polarization in the free layer and hence lower the critical switching current [12]. Other implications such as magnetization oscillations due to spin-torque effects within the noncollinear reference system might introduce further implications for the device optimization.

This paper is organized as follows. In Sec. II we provide an overview of the effect of noncollinear coupling and the concept of bilinear and biquadratic coupling constants.

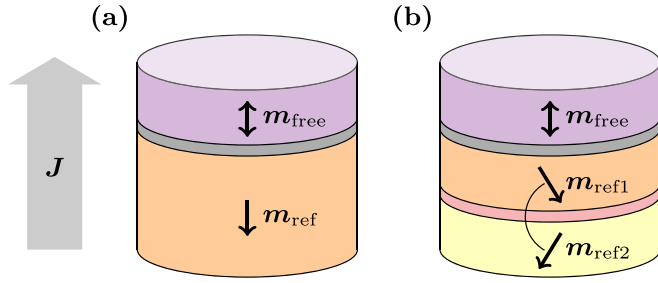*claas.abert@univie.ac.at
†sabri.koraltan@univie.ac.at

FIG. 1. Simplified perpendicular MRAM stack with magnetic free layer m_{free} and magnetic reference layer m_{ref}. When applying a perpendicular current, J, the reference layer polarizes the itinerant electrons, resulting in a spin torque exerted on the free-layer magnetization. (a) Conventional collinear MRAM. (b) MRAM with noncollinear reference system for improved writing.

Furthermore, we discuss the shortcomings of existing modeling approaches in order to motivate the development of the presented model. In Sec. III we introduce an atomistic model to explain the origin of noncollinear coupling, and in Sec. IV we explain how we use numerical simulation to solve the presented model. In Sec. V we present simulation results for various systems, and we compare them to experimental data from our previous publication [21]. In Sec. VI we validate the predictions made by our model with experimental measurements. The conclusion is given in Sec. VII.

II. NONCOLLINEAR COUPLING

In [21], we developed a simple micromagnetic model based on a fluctuation mechanism introduced in [22] that divides the spacer layer laterally into regions of ferromagnetic coupling and antiferromagnetic coupling. In this model, the coupling energy across the RuFe spacer layer is given by the interface integral

$$E = \int_{\Gamma} -A(x) m_1(x) \cdot m_2(x) ds, \qquad (1)$$

with Γ being the interface between the magnetic layers, m_1 and m_2 being the respective magnetization configurations in these layers, and A being the spatially varying coupling constant. If the spatial fluctuations in A are on a lengthscale L_{fluc} that is small compared to the exchange length L_{ex} of the ferromagnetic layers, $L_{\text{fluc}} \ll L_{\text{ex}}$, the effective coupling of the magnetization in the ferromagnetic layers m_1 and m_2 amounts to the average coupling constant $\bar{A}$, resulting in an areal energy density

$$\epsilon = -\bar{A} m_1 \cdot m_2 \qquad (2)$$

and collinear coupling of the ferromagnetic layers. If L_{fluc} is large compared to L_{ex}, the ferromagnetic layers will couple region by region, leading to a domain pattern defined by the distribution of ferromagnetically ($A > 0$) and antiferromagnetically ($A < 0$) coupled regions. However, if $L_{\text{fluc}} \approx L_{\text{ex}}$, the fluctuations in the coupling constant are able to generate slight inhomogeneities in the ferromagnetic layers without generating domains. In this case, the magnetization in the ferromagnetic layers can be assumed to be approximately homogeneous, and the coupling of the ferromagnetic layers
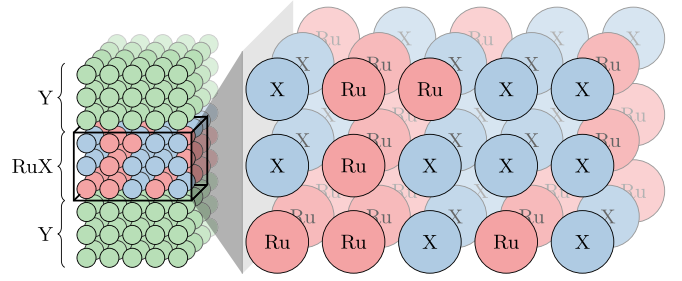

FIG. 2. Atomistic model of ferromagnetic multilayer structure, with the alloy spacer layer containing ferromagnetic (X/Y) as well as Ru atoms in a cubic lattice.

can be described by adding an additional biquadratic term to the coupling energy,

$$\epsilon = -A_1 m_1 \cdot m_2 - A_2 (m_1 \cdot m_2)^2. \qquad (3)$$

The values of A_1 and A_2 depend on various system parameters such as the exchange constant of the ferromagnetic layers and the exact distribution of the coupling strength $A(x)$. For negative A_2 and $|A_1| < |2A_2|$, noncollinear coupling of the ferromagnetic layers becomes energetically stable. To theoretically determine the macroscopic coupling constants A_1 and A_2, a microscopic model that resolves the inner structure of the spacer layer is required. While the micromagnetic model based on lateral fluctuations in $A(x)$ has been shown to provide a possible explanation for the noncollinear coupling in Co/RuFe/Co multilayers [21], it fails to accurately describe all experimentally observed effects of the coupling mediated by RuFe layers. For instance, the A_1 as predicted by the micromagnetic model exhibits a linear dependence on the fraction of Ru content in the spacer layer, while the experiment shows saturation for high Ru content [21]. This leads to unrealistically high values of A_1 when fitting the model parameters to reproduce the experimentally observed A_2. Moreover, the micromagnetic model has a low predictivity for the dependence of A_1 and A_2 on the spacer-layer thickness since it requires the thickness-dependent antiferromagnetic coupling constant as an input.
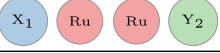
III. MODEL

To overcome the weaknesses of the micromagnetic model, we employ a simple atomistic model that considers pair coupling of neighboring ferromagnetic atoms as well as indirect coupling of ferromagnetic atoms across Ru atoms. For the sake of simplicity, we assume a cubic lattice where each atomic site is either populated by a ferromagnetic atom X/Y or a Ru atom; see Fig. 2. For neighboring ferromagnetic atoms in the principal directions of the cubic lattice, we employ the classical Heisenberg model

$$\mathcal{H} = -J S_1 \cdot S_2, \qquad (4)$$

with J being the coupling constant and S_1 and S_2 being unit vectors that represent the coupled spins. To account for the influence of the Ru atoms in the spacer layer, we assume that the ferromagnetic atoms are also coupled when separated by one or more Ru atoms in one of the three principal directions

TABLE I. Exemplary couplings of ferromagnetic atoms depending on neighboring Ru atoms. The couplings are generalized up to arbitrary distances and applied along all three principal axes.

Type	Energy
X_1 X_2	$E = -J_1^{X/X} m_{X_1} \cdot m_{X_2}$
X_1 Y_2	$E = -J_1^{X/Y} m_{X_1} \cdot m_{Y_2}$
Y_1 Y_2	$E = -J_1^{Y/Y} m_{Y_1} \cdot m_{Y_2}$
X_1 Ru X_2	$E = -J_2^{X/Ru/X} m_{X_1} \cdot m_{X_2}$
…	
X_1 Ru Ru Y_2	$E = -J_3^{X/Ru/Y} m_{X_1} \cdot m_{Y_2}$
…	

of the lattice; see Table I. The Hamiltonian of our atomistic model is completed by the Zeeman energy and a uniaxial anisotropy that accounts for both crystalline as well as shape anisotropy, resulting in

$$\mathcal{H} = -\sum_{i,j} J_{k(i,j)} S_i \cdot S_j - \sum_i \mu_0 \mu_i H \cdot S_i + K a^3 (S_i \cdot e_k)^2, \tag{5}$$

with $J_{k(i,j)}$ being the coupling constant according to Table I, μ_i being the magnetic moment of a single atom, K being the anisotropy constant, and e_k being the unit vector along the uniaxial anisotropy axis. The coupling constants J_k for the atomistic model can be determined from micromagnetic constants that can be determined by measurement. The nearest-neighbor coupling J_1 is chosen as $J_1 = A_{ex} a$, with A_{ex} being the exchange constant and a being the (artificial) cubic lattice constant in order to reproduce accurate ferromagnetic behavior in homogeneous layers. The coupling constants J_k with $k > 1$ can be chosen according to the areal interlayer exchange coupling strength of multilayers with pure Ru spacer layers, $A(d)$, with layer thickness d as $J_k = A(ka)a^2$ [23]. By this gauge process, the atomistic model is equivalent to a micromagnetic model for simple systems such as ferromagnetic monolayers or ferromagnetic layers separated by pure Ru layers of arbitrary thickness.

The assumption of a cubic lattice along with the restriction of couplings along the principal directions remains to be one of the main simplifications introduced by the presented model since many ferromagnetic as well as alloyed materials exhibit more complicated lattice structures [24–26]. The choice of the cubic lattice constant a applies to all involved materials and hence always constitutes a compromise. Changes in a will impact the quantitative results of the model, even if all involved coupling parameters are scaled accordingly.

IV. SIMULATION

To find stable magnetization configurations for arbitrary spacer-layer compositions, we minimize (5) with respect to the spin configuration S_i, considering the unit sphere constraint $|S_i| = 1$. With this minimization procedure, the equilibrium magnetization configuration and the angle between the ferromagnetic layers can be obtained. To determine the macroscopic coupling constants A_1 and A_2 for a specific spacer-layer configuration, the equilibrium spin configuration for various in-plane external fields H is determined for a symmetric system with two identical ferromagnetic layers with an effective easy-plane anisotropy. In this configuration, the magnetization in the ferromagnetic layers can be considered symmetric around the field direction. This means that $m_1 \cdot e_{field} = m_2 \cdot e_{field} = \cos(\theta/2)$, with e_{field} being the direction of the in-plane external field and θ being the angle between the macroscopic magnetizations $\cos(\theta) = m_1 \cdot m_2$. With this choice of field and anisotropy, the areal energy density of the system only depends on the angle θ and reads

$$\epsilon(\theta) = -A_1 \cos(\theta) - A_2 \cos^2(\theta)$$
$$- 2d_{fm}[H\mu_0 M_s \cos(\theta/2) + K \sin^2(\theta/2)], \tag{6}$$

with d_{fm} being the thickness of the ferromagnetic films. The macroscopic coupling constants A_1 and A_2 can then be determined from atomistic simulations by fitting simulated values of θ to the equilibrium energy density condition $d\epsilon/d\theta(H, A_1, A_2) = 0$. The atomistic model is benchmarked against the experimental findings for the Co/RuFe/Co multilayer introduced in [21]. As a lattice constant, we choose $a = 0.23$ nm throughout the complete system. To accurately account for the exchange coupling within the ferromagnetic layers, we compute the Heisenberg exchange constants J_1 from the respective exchange constants A_{ex} as $J_1 = Aa$. Namely, we use $J_1^{Co/Co} = 6 \times 10^{-21}$ J and $J_1^{Co/Fe} = J_1^{Fe/Fe} = 4.5 \times 10^{-21}$ J. The dipole moments of our model μ are obtained from the saturation magnetization M_s as $\mu = M_s a^3$. For the sake of simplicity, we set $\mu^{Co} = \mu^{Fe} = 2.11\mu_B$. To account for the dipole-dipole interaction, we introduce an effective anisotropy in the Co layers that accounts for both the crystalline as well as the shape anisotropy, $K_{eff} = K_{cryst} - \mu_0 M_s^2/2 = -7.1 \times 10^5$ J/m^3; see [21]. The shape anisotropy is chosen as easy-plane anisotropy of an infinite plane with a demagnetizing factor of 1, which is a reasonable choice for the extended thin films investigated in [21]. For the (antiferromagnetic) coupling across Ru atoms, we choose $J_k^{Fe/Ru/Fe} = -1.85 \times 10^{-40}$ Jm^2/$(ka)^2$, $J_k^{Co/Ru/Fe} = -2.38 \times 10^{-40}$ Jm^2/$(ka)^2$, and $J_k^{Co/Ru/Co} = -7.94 \times 10^{-40}$ Jm^2/$(ka)^2$. We consider only couplings across up to four Ru atoms, which justifies the simplified dependence on the distance ka. While the coupling mediated by Ru atoms is usually expected to oscillate and change sign with the distance, a purely antiferromagnetic coupling with a decay of $1/(ka)^2$ is in agreement with the experimental data on Co/Ru/Co multilayers reported in [21] and has proven to yield good macroscopic results. However, depending on the exact material system under consideration, the presented model can easily be adjusted to model an arbitrary dependence of the Ru-mediated coupling from the distance. The distribution of ferromagnetic (Fe) and nonmagnetic (Ru) atoms in the spacer layer is randomly generated according to the respective composition.

To find stable magnetization configurations, we use a random configuration as an initial value and apply an adaptive steepest-descent minimizer to the energy functional
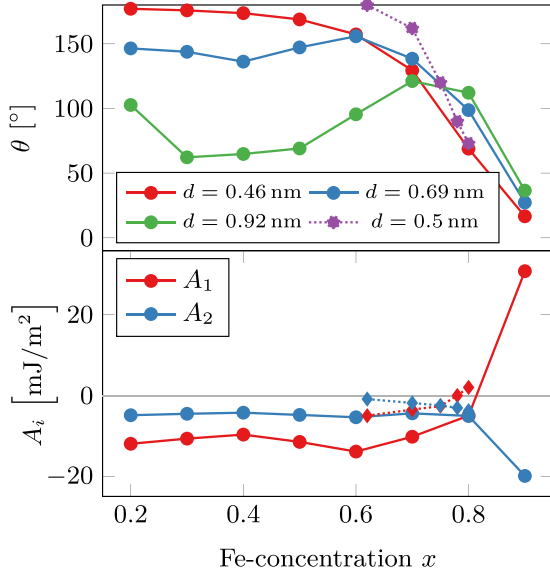
FIG. 3. Equilibrium angle θ and macroscopic coupling constants A_1 and A_2 for a Co/RuFe/Co multilayer system for various Fe concentrations x in the spacer layer. Simulations for θ were performed for various spacer-layer thicknesses given in atomic layers n_z. Simulations for A_1 and A_2 were performed for $n_z = 3$. The dotted lines mark experimental values for a spacer-layer thickness of $d = 0.5$ nm; see [21].

(5). Specifically, we use a pseudotransient method that considers the unit sphere constraint of the spins. For this purpose, we introduce an effective field

$$\boldsymbol{H}_{\mathrm{eff},i} = -\frac{\partial \mathcal{H}}{\partial \boldsymbol{S}_i} \qquad (7)$$

and solve the time-dependent differential equation

$$\frac{\partial \boldsymbol{S}_i}{\partial t} = -\boldsymbol{S}_i \times (\boldsymbol{S}_i \times \boldsymbol{H}_{\mathrm{eff},i}) \qquad (8)$$

with an adaptive, explicit Runge-Kutta method to find a stable solution. This procedure is equivalent to a projected steepest-descent method in the tangential plane of $\boldsymbol{S}_i$ [27] and hence is suitable for the minimization of $\boldsymbol{S}_i$ subject to the unit-sphere constraint. The numerical implementation is done with PyTorch [28], enabling fast simulation on graphics processing units (GPUs).

V. RESULTS

We perform simulations of the Co/RuFe/Co system introduced in [21] in order to compare and validate our model against the experimental results published therein. Figure 3 shows the simulation results for varying Fe concentrations in the spacer layer. The simulated system has a lateral size of 40×40 spins and layer thicknesses of 10 atomic layers for each of the two Co layers. This system size turned out to be sufficient to average out the influence of the random distribution of atoms in the spacer layer to a negligible level. We calculate the equilibrium coupling angle of the Co layers for various Fe concentrations and thicknesses of the spacer RuFe layer, and we compare to experimental findings for a 0.5 nm spacer layer, which equals two to three atomistic layers in our
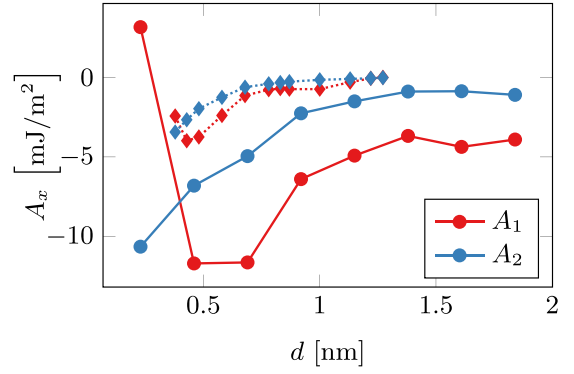

FIG. 4. Bilinear and biquadratic coupling constants A_1 and A_2 in $Co/Ru_{30}Fe_{70}/Co$ multilayer depending on the thickness of the spacer layer as measured in [21] (dotted lines) and simulated with the atomistic model (solid lines).

simplified model; see Fig. 3, top panel. The simulated results show a good agreement, specifically with respect to the slope of angle that describes a smooth transition from antiferromagnetic to ferromagnetic coupling around a Fe concentration of 0.7. For a larger spacer-layer thickness of four atomic layers, the simulated equilibrium angle θ exhibits a notable dip around $x = 0.4$ that is not seen in experiment. We attribute this deviation to the simplifications of our model, such as the assumption of a cubic lattice. Furthermore, we compute the macroscopic coupling constants A_1 and A_2 for various Fe concentrations for a fixed spacer-layer thickness of three atomic layers; see Fig. 3, bottom panel. While the simulations in this case fail to accurately reproduce the experimental values in a quantitative fashion, they perfectly reproduce notable trends seen in experiment. Namely, the bilinear coupling constant A_1 saturates for low Fe concentrations, and the biquadratic coupling constant A_2 decreases slightly in the significant coupling region around $x = 0.7$. We use the same simulation procedure to calculate the thickness dependence of A_1 and A_2 on the spacer-layer thickness for a fixed Fe concentration of $x = 0.7$, which marks exactly the center of the transition between antiferromagnetic and ferromagnetic coupling, see Fig. 4. As for previous simulation results, the presented model fails to quantitatively match the experimental measurements, but it shows an excellent agreement concerning the trends. For intermediate to high spacer-layer thicknesses d, both A_1 and A_2 are negative with asymptotically decreasing magnitude and $A_1 < A_2$. At $d \approx 0.5$ nm, both simulation and experiment exhibit a dip in the bilinear coupling constant A_1 and a crossing of A_1 and A_2, which constitutes a great agreement. To compute the magnetic moment of the spacer layer depending on spacer-layer thickness and Fe concentration, the system is relaxed to an energetic minimum at zero external field. We compute the averaged moment of the spacer layer in relative units of the Fe saturation magnetization by summing up the normalized spins of all ferromagnetic atoms in the spacer layer N_{mag}, and we divide by the total number of atoms in the spacer layer N_{all},

$$\langle \boldsymbol{m} \rangle = N_{\mathrm{all}}^{-1} \sum_{i \in N_{\mathrm{mag}}} \boldsymbol{s}_i. \qquad (9)$$
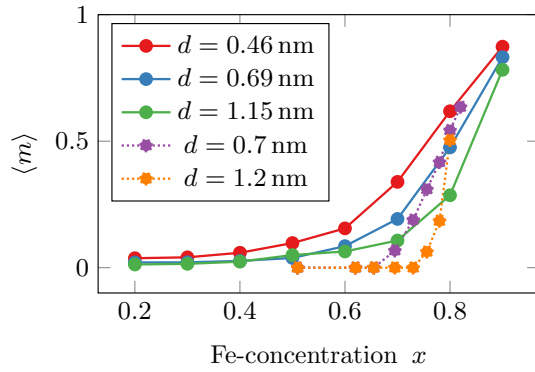
FIG. 5. Relative saturation of spacer-layer magnetization (1 means full Fe saturation) depending on Fe concentration and spacer layer thickness. Solid lines represent simulation results with layer thicknesses given in number of atomic layers n_z, and dotted lines represent experimental data [21] with layer thicknesses d.

Instead of a linear behavior $\langle m \rangle \propto x$ that would be expected for uncoupled Fe atoms, the magnetic moment of the spacer layer almost vanishes for $x < 0.5$ and shows steep ascent around the critical Fe concentration 0.7, which reproduces the experimental findings, see Fig. 5. As for the experimental measurements, the simulations show a steeper transition for larger spacer-layer thicknesses. To understand the highly nonlinear dependence of the spacer-layer magnetization from the Fe concentration, the spin configuration is investigated in detail. Figure 6(a) depicts the equilibrium configuration for a multilayer with a spacer-layer thickness of five atomic layers. As indicated by the streamlines, the spacer-layer magnetization exhibits a nontrivial magnetization configuration with multiple vortexlike structures. This misalignment of spins in the spacer layer explains the asymptotic behavior of the net magnetization for high-layer thicknesses. The magnetic vortices are obviously caused by the complicated interplay of couplings between the ferromagnetic atoms within the spacer layer, including ferromagnetic and antiferromagnetic couplings.

Note that the spacer-layer spins at the interfaces to the magnetic layers are almost homogeneous. The tilting of the bottom and top magnetic layers seems to be caused by a complex transition of the magnetic spins within the spacer layer. This kind of coupling mechanism is fundamentally different from the micromagnetic model proposed by Slonczewski and used in our former work. In the micromagnetic model, the ferromagnetic regions of the spacer layer are basically assumed to be rigid, and the noncollinearity is merely a result of the alternating ferromagnetic and antiferromagnetic coupling that results in slight fluctuations in the magnetization configuration of the ferromagnetic layers [21]. Hence, the stability of noncollinear states as described by the Slonczewski model is highly dependent on the exchange constant of the ferromagnetic layers A and vanishes for infinite stiffness since $A_2 \propto 1/A_{\mathrm{ex}}$. The proposed atomistic model, however, enables noncollinear coupling even for infinitely stiff ferromagnetic layers, since the noncollinearity evolves within the spacer layer itself, as shown in Fig. 6. To investigate the influence of the exchange constant, we compute the equilibrium angle of
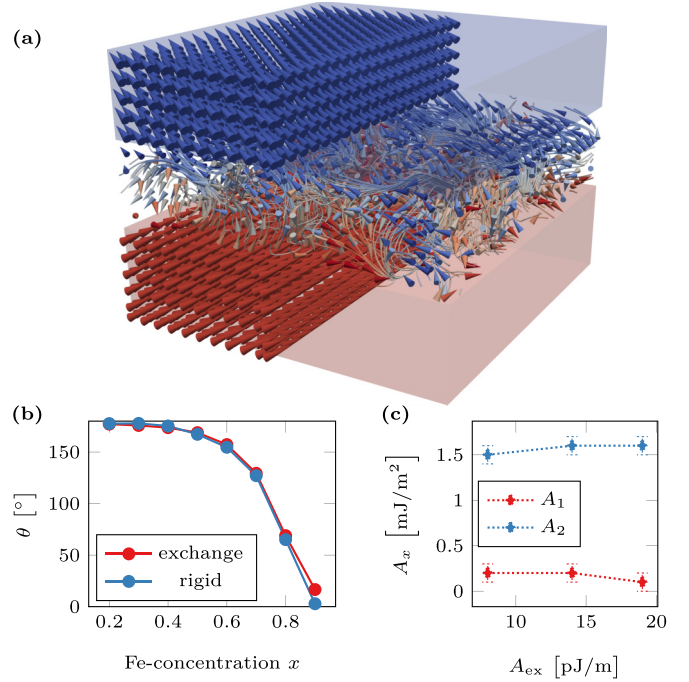

FIG. 6. (a) Noncollinear magnetization configuration of a magnetic multilayer with rigid ferromagnetic layers and a spacer-layer thickness of five atomic layers. (b) Simulated equilibrium magnetization angle for various Fe concentrations for ferromagnetic layers with realistic exchange coupling (exchange) compared to infinitely stiff ferromagnetic layers (rigid) for a spacer-layer thickness of two atomic layers. (c) Bilinear and biquadratic coupling constants A_1 and A_2 in a Co/RuFeCo/Co multilayer depending on the exchange stiffness A_{ex} in the ferromagnetic layers.

the magnetization for a realistic exchange stiffness within the ferromagnetic layers, and we compare the result with a similar three-layer structure having infinitely stiff ferromagnetic layers. The results shown in Fig. 6(b) demonstrate the negligible influence of the exchange stiffness of the ferromagnetic layers on the simulation outcome.

VI. EXPERIMENTS

To check the independence of the noncollinear coupling from the exchange stiffness of the ferromagnetic Co layers, we perform additional experiments. Namely, we perform measurements on a Co/RuFeCo/Co multilayer where we artificially reduce the exchange stiffness in the Co layers by doping. For this purpose, we fabricate Ta(3.5)/Ru(3.5)/Co$_{100-x}$Ru$_x$(5.2)/Co(0.8)/Ru$_{33.4}$(Fe$_{50}$Co$_{50}$)$_{66.5}$/Co(0.8)/Co$_{100-x}$Ru$_x$(5.2)Ru$_{3.5}$ multilayers, where the values in parentheses denote the respective layer thicknesses in nm and x denotes the Ru concentration in the CoRu layers. The magnetic layers in the deposited structure consist of a thick Co$_{100-x}$Ru$_x$ layer and a thin Co interface layer. The role of the Co interface layer is to ensure that the coupling between the magnetic layers (Co$_{100-x}$Ru$_x$/Co) across the RuFeCo spacer layer is not affected by the Ru concentration in Co$_{100-x}$Ru$_x$ [29]. The exchange stiffness of the Co$_{100-x}$Ru$_x$/Co magnetic layer is modified by varying the Ru concentration in the thick Co$_{100-x}$Ru$_x$ layer. Eyrich

et al. showed that adding Ru to Co can sharply decrease the exchange stiffness of Co [30]. We deposit multilayers with radiofrequency magnetron sputtering on (100) Si substrates at room temperature and an argon pressure below 2 mTorr. The Ta seed layer is deposited to induce the growth orientations of the Ru, CoRu, Co, and RuFeCo layers, and the top Ru film is used to protect magnetic layers from oxidation. For details regarding the substrate cleaning and film deposition, see [21]. Figure 6(c) shows the dependence of A_1 and A_2 on the exchange stiffness in $Co_{100-x}Ru_x$/Co magnetic layers. It is evident that A_1 and A_2 are independent of A_{ex}, which confirms the prediction made by our model.

VII. CONCLUSION

In conclusion, we present an atomistic model for the description of magnetic multilayer structures with spacer layers made from Ru alloyed to ferromagnetic material. Our model accounts for the influence of the Ru atoms by means of additional Heisenberg coupling terms that couple magnetic atoms separated by Ru atoms in an antiferromagnetic fashion. We find that the proposed model is able to reproduce the experimental results to a high level of detail, which is not accomplished by the micromagnetic model of Slonczewski that was used in our former publications [21]. Our model is able to correctly describe trends with respect to the change of composition and thickness of the spacer layer, and it predicts noncollinear coupling even for infinitely stiff ferromagnetic layers. Quantitative deviations can be attributed to simplifications introduced by the model, e.g., the assumption of a cubic lattice and the restriction of couplings to the principal directions of the lattice. The prediction of a noncollinear coupling, which is largely independent from the exchange stiffness of the ferromagnetic layers, has been validated experimentally. This is expected to have tremendous implications on the future development of spintronic devices with noncollinear coupling.

[1] C. Zheng, K. Zhu, S. Cardoso de Freitas, J.-Y. Chang, J. E. Davies, P. Eames, P. P. Freitas, O. Kazakova, C. Kim, C.-W. Leung, S.-H. Liou, A. Ognev, S. N. Piramanayagam, P. Ripka, A. Samardak, K.-H. Shin, S.-Y. Tong, M.-J. Tung, S. X. Wang, S. Xue *et al.*, IEEE Trans. Magn. **55**, 1 (2019).

[2] B. Dieny, I. L. Prejbeanu, K. Garello, P. Gambardella, P. Freitas, R. Lehndorff, W. Raberg, U. Ebels, S. O. Demokritov, J. Akerman, A. Deac, P. Pirro, C. Adelmann, A. Anane, A. V. Chumak, A. Hirohata, S. Mangin, S. O. Valenzuela, M. C. Onbaşlı, M. d'Aquino *et al.*, Nat. Electron. **3**, 446 (2020).

[3] J. S. Meena, S. M. Sze, U. Chand, and T.-Y. Tseng, Nanoscale Res. Lett. **9**, 526 (2014).

[4] Y.-C. Lau, D. Betto, K. Rode, J. M. D. Coey, and P. Stamenov, Nat. Nanotechnol. **11**, 758 (2016).

[5] S. Bhatti, R. Sbiaa, A. Hirohata, H. Ohno, S. Fukami, and S. Piramanayagam, Mater. Today **20**, 530 (2017).

[6] T. Kosub, M. Kopte, R. Hühne, P. Appel, B. Shields, P. Maletinsky, R. Hübner, M. O. Liedke, J. Fassbender, O. G. Schmidt, and D. Makarov, Nat. Commun. **8**, 13985 (2017).

[7] N. Sato, F. Xue, R. M. White, C. Bi, and S. X. Wang, Nat. Electron. **1**, 508 (2018).

[8] V. E. Demidov, S. Urazhdin, H. Ulrichs, V. Tiberkevich, A. Slavin, D. Baither, G. Schmitz, and S. O. Demokritov, Nat. Mater. **11**, 1028 (2012).

[9] T. Chen, R. K. Dumas, A. Eklund, P. K. Muduli, A. Houshang, A. A. Awad, P. Durrenfeld, B. G. Malm, A. Rusu, and J. Akerman, Proc. IEEE **104**, 1919 (2016).

[10] C. Safranski, I. Barsukov, H. K. Lee, T. Schneider, A. A. Jara, A. Smith, H. Chang, K. Lenz, J. Lindner, Y. Tserkovnyak, M. Wu, and I. N. Krivorotov, Nat. Commun. **8**, 117 (2017).

[11] M. A. Ruderman and C. Kittel, Phys. Rev. **96**, 99 (1954).

[12] Y. Zhou, S. Bonetti, C. L. Zha, and J. Åkerman, New J. Phys. **11**, 103028 (2009).

[13] N. N. Mojumder and K. Roy, IEEE Trans. Electron. Devices **59**, 3054 (2012).

[14] R. Law, E.-L. Tan, R. Sbiaa, T. Liew, and T. C. Chong, Appl. Phys. Lett. **94**, 062516 (2009).

[15] R. Sbiaa, J. M. Shaw, H. T. Nembach, M. Al Bahri, M. Ranjbar, J. Åkerman, and S. N. Piramanayagam, J. Phys. D **49**, 425002 (2016).

[16] A. D. Kent, B. Özyilmaz, and E. del Barco, Appl. Phys. Lett. **84**, 3897 (2004).

[17] D. Suess, C. Vogler, F. Bruckner, H. Sepehri-Amin, and C. Abert, Appl. Phys. Lett. **110**, 252408 (2017).

[18] Y. Zhou, C. L. Zha, S. Bonetti, J. Persson, and J. Åkerman, Appl. Phys. Lett. **92**, 262508 (2008).

[19] W. Skowroński, T. Stobiecki, J. Wrona, G. Reiss, and S. V. Dijken, Appl. Phys. Express **5**, 063005 (2012).

[20] R. Arun, R. Gopal, V. K. Chandrasekar, and M. Lakshmanan, J. Appl. Phys. **127**, 153903 (2020).

[21] Z. R. Nunn, C. Abert, D. Suess, and E. Girt, Sci. Adv. **6**, eabd8861 (2020).

[22] J. C. Slonczewski, Phys. Rev. Lett. **67**, 3172 (1991).

[23] T. McKinnon, B. Heinrich, and E. Girt, Phys. Rev. B **104**, 024422 (2021).

[24] J. Kim, R. Ramesh, and N. Kioussis, Phys. Rev. B **94**, 180407 (2016).

[25] C. Bordel, J. Juraszek, D. W. Cooke, C. Baldasseroni, S. Mankovsky, J. Minár, H. Ebert, S. Moyerman, E. E. Fullerton, and F. Hellman, Phys. Rev. Lett. **109**, 117201 (2012).

[26] M. Wolloch, M. E. Gruner, W. Keune, P. Mohn, J. Redinger, F. Hofer, D. Suess, R. Podloucky, J. Landers, S. Salamon, F. Scheibel, D. Spoddig, R. Witte, B. Roldan Cuenya, O.

Gutfleisch, M. Y. Hu, J. Zhao, T. Toellner, E. E. Alp, M. Siewert *et al.*, Phys. Rev. B **94**, 174435 (2016).

[27] C. Abert, Eur. Phys. J. B **92**, 120 (2019).

[28] A. Paszke, S. Gross, F. Massa, A. Lerer, J. Bradbury, G. Chanan, T. Killeen, Z. Lin, N. Gimelshein, L. Antiga *et al.*, Adv. Neural Inf. Process. Syst. **32**, 8026 (2019).

[29] M. Arora, N. R. Lee-Hone, T. Mckinnon, C. Coutts, R. Hübner, B. Heinrich, D. M. Broun, and E. Girt, J. Phys. D **50**, 505003 (2017).

[30] C. Eyrich, A. Zamani, W. Huttema, M. Arora, D. Harrison, F. Rashidi, D. Broun, B. Heinrich, O. Mryasov, M. Ahlberg, O. Karis, P. E. Jönsson, M. From, X. Zhu, and E. Girt, Phys. Rev. B **90**, 235408 (2014).